Multi-azimuth Prestack Time Migration for General Anisotropic, Weakly Heterogeneous Media - Field Data Examples

S. Beaumont* (EOST/PGS) & W. Söllner (PGS)

SUMMARY

Multi-azimuth data acquisition has shown benefits in noise reduction and structure illumination, which leads generally to improved seismic images. However the current time processing, which is based on independent processing of the data from the different predominant azimuths, may lead to destructive interferences and deterioration of the final stacked image when the earth model is anisotropic or laterally heterogeneous. In order to solve this problem a prestack time migration for anisotropic, weakly heterogeneous media has been recently introduced and tested on synthetic data. In this work, we ran a first field data application on a multi-azimuth data set. From data in three different acquisition azimuths we performed migration velocity analysis to build azimuth-dependent migration operators. We processed the data in parallel also with conventional narrow azimuth prestack time migration in order to assess the performance of the new approach.

Introduction

Acquisition of data over the same area with different azimuths (multi-azimuth data acquisition) allows building stacked volumes with better signal to noise ratio and generally improved target illumination (e.g., Manning et al., 2007). However, the current time processing is not sufficiently adapted to this data acquisition approach. Indeed, data from different predominant azimuthal directions are processed independently, with azimuthally independent time velocity functions, and are combined (stacked together) only at the very last imaging step. As a consequence, one and the same image point in general heterogeneous and anisotropic media may be placed at different time positions for different azimuths, which may lead to destructive interferences and a deterioration of the image. In order to extend prestack time migration to anisotropic and weakly heterogeneous media, a new method for multi-azimuth prestack time migration (MAPSTM) has been developed (e.g., Söllner et al., 2010). This method allows computing the azimuthal diffraction time functions necessary to build the diffraction stack using the most general form of Hamilton's principal equation. Starting from conventional narrow-azimuth prestack time migrations and velocity analysis on data for at least three independent azimuths, time migration velocity ellipses can be build, and subsequently the azimuthal diffraction time functions calculated. This method, previously tested on synthetic data, is in this work for the first time tested and successfully applied on a multi-azimuth data example acquired in the Nile Delta in 2003.

Theory

Multi-azimuth prestack time migration: The migration used in this method is a Kirchhoff-type migration, which consists of summing (in the input data space) the amplitudes along the diffraction time function for the endpoint of a given image ray, and placing this sum (in the output data space) onto the two-way time and the surface position of that image ray. Thus, to perform this migration, the diffraction time function is required for all the surface grid points of the output data space at all relevant two-way times.

We assume the subsurface is well modeled by a pile of anisotropic weakly heterogeneous layers separated by arbitrarily dipping, smoothly curved interfaces. We assume further that traveltimes of transmitted rays are with sufficient accuracy expressed by second order approximations around one selected image ray (considered as central ray), and build the traveltime of transmitted rays using Hamilton's point characteristic (Buchdahl, 1970; Bortfeld, 1989; Moser and Červený, 2007; Söllner et al., 2010):

$$t_{\mathbf{r}}(\mathbf{x}_{\mathbf{r}},\mathbf{x}'=\mathbf{0}) = t_0 + \frac{1}{2}\mathbf{x}_{\mathbf{r}} \cdot \mathbf{B}_0^{-1}\mathbf{A}_0\mathbf{x}_{\mathbf{r}} \tag{1}$$

The one-way traveltimes $t_{\mathbf{r}}(\mathbf{x_r},\mathbf{x'=0})$ for any transmitted ray starting at the receiver position $\mathbf{x_r}$ (at the surface) and ending at $\mathbf{x'=0}$ (the endpoint of the central ray) are calculated in equation 1 from the exact traveltime along the central ray, t_0, and the 2x2 surface-to-surface paraxial matrices $\mathbf{A_0}$ and $\mathbf{B_0}$. The elements of the surface-to-surface paraxial matrices (Bortfeld, 1989) are commonly obtained from dynamic ray tracing for given model parameters (Hubral et al., 1992; Červený, 2001).

A better approximation of the transmitted times are achieved by squaring on both sides of equation 1 and dropping the terms of power higher than two:

$$t_{\mathbf{r}}^2(\mathbf{x}_{\mathbf{r}},\mathbf{x}'=\mathbf{0}) = t_0^2 + t_0\mathbf{x}_{\mathbf{r}} \cdot \mathbf{B}_0^{-1}\mathbf{A}_0\mathbf{x}_{\mathbf{r}}\,. \tag{2}$$

The traveltime expression in equation 2 is a hyperbolic approximation of $t_{\mathbf{r}}$ (Ursin, 1982). Moreover, as the matrix combination $\mathbf{B_0}^{-1}\mathbf{A_0}$ is a symmetric 2x2 matrix, it can be replaced in equation 2 by its three (unknown) components denoted as U_{11}, U_{12}, U_{22}. The receiver position vector can also be expressed by its azimuth (angle between receiver position vector and x-axis) and the distance, $d_{\mathbf{r}}$, between the receiver and the image ray. Hence, the traveltime $t_{\mathbf{r}}$ can now be written as

$$t_{\mathbf{r}}^2 = t_0^2 + \frac{d_{\mathbf{r}}^2}{V_{TM}(\alpha_{\mathbf{r}})^2}\,, \tag{3}$$

with

$$V_{TM}(\alpha_{\mathbf{r}})^{-2} = t_0\{U_{11}\cos^2(\alpha_{\mathbf{r}}) + 2U_{12}\cos(\alpha_{\mathbf{r}})\sin(\alpha_{\mathbf{r}}) + U_{22}\sin^2(\alpha_{\mathbf{r}})\}. \quad (4)$$

$V_{TM}(\alpha_{\mathbf{r}})$ represents the time migration velocity ellipse. Although equations 3 and 4 have formal similarity with the NMO velocity derived by Grechka and Tsvankin (1999), the azimuth angle has different meaning here (it is not related to the acquisition azimuth) and V_{NMO} and V_{TM} are equal solely in the trivial case when the image rays and the normal rays are identical.

After repeating above derivation for the transmitted ray from any source at the surface to the end point of the central ray and summing the two traveltimes, we obtain the complete diffraction time function of a diffraction point at the endpoint of the image ray:

$$t_{TM} = \sqrt{t_0^2 + \frac{d_{\mathbf{r}}^2}{V_{TM}(\alpha_{\mathbf{r}})^2}} + \sqrt{t_0^2 + \frac{d_{\mathbf{s}}^2}{V_{TM}(\alpha_{\mathbf{s}})^2}}\,. \quad (5)$$

Prestack time-migration using the diffraction time function t_{TM} from equation 5 generates flat offset panels in all azimuthal directions only if the V_{TM} ellipse is correct. As a consequence one can replace the dynamic ray tracing by trial multi-azimuth prestack time migrations to determine the diffraction time function.

Azimuthal velocity analysis: As the depth model needed for ray tracing is generally not known at time processing stage, replacing ray tracing by trial time migrations followed by velocity analysis has an obvious advantage. Looking for a practical approach for velocity analysis, we derive the diffraction time function after expressing in equation 1 the receiver position vector, **r**=**m**+**h,** by midpoint **m** and half offset **h** vectors. Following Hubral and Krey (1980), we obtain

$$t_D(\mathbf{m},\mathbf{h}) = 2t_0 + \mathbf{m}\cdot\mathbf{B}_0^{-1}\mathbf{A}_0\mathbf{m} + \mathbf{h}\cdot\mathbf{B}_0^{-1}\mathbf{A}_0\mathbf{h}\,. \quad (6)$$

The hyperbolic approximation with inserted V_{TM} from equation 4, with $d_{\mathbf{m}}=|\mathbf{m}|$, and $d_{\mathbf{h}}=|\mathbf{h}|$, becomes

$$t_D(\mathbf{m},\mathbf{h})^2 = 4t_0^{\,2} + 4d_{\mathbf{m}}^{\,2}/V_{TM}(\alpha_{\mathbf{m}})^2 + 4d_{\mathbf{h}}^{\,2}/V_{TM}(\alpha_{\mathbf{h}})^2\,. \quad (7)$$

The diffraction time function $t_D(\mathbf{m},\mathbf{h})$ in equation 7 is because of its separation in midpoint and offset dependent moveout terms a suitable expression for V_{TM} updating in a velocity analysis scheme.

A first trial migration of common offset panels (using equation 5), on one predominant azimuth, with non-azimuthal velocities will most probably result into non-flat image gathers. As $d_{\mathbf{m}}$ goes to zero for a migrated image point, the remaining offset dependent moveout term in equation 7 is added using the same trial velocity. Subsequently, velocity analysis is applied to flatten the image gather, again using only the offset dependent term in equation 7. This procedure gives an updated velocity field for the azimuth $\alpha_{\mathbf{h}}$, and from at least three independent predominant azimuth directions the updated V_{TM} ellipse is reconstructed.

Field data example

The data was acquired during a multi-azimuth survey in the Nile Delta, in deep water (Keggin et al., 2007; van der Burg et al., 2010). This area is characterized by a complex water bottom and shallow channel systems made of gas hydrates, above the Messinian. The complex layer, which appears as a strong reflector around three seconds in the seismic data, is composed of marine sediments and anhydrite deposits.

Six azimuths were acquired, every thirty degrees. But for this study only three different predominant azimuths were available: the azimuths 60°, 120° and 150°. The data for each azimuth were pre-processed to remove multiples, and then (after azimuthal velocity analysis) migrated with both a multi-azimuth prestack time migration (MAPSTM) and a narrow-azimuth prestack time migration (NAPSTM), in order to assess the performance of the new method.

We will now compare the results from the narrow-azimuth and multi-azimuth prestack time migrations, for the case where the three available azimuths have been combined. Figure 1-a shows a zoom on the stacked volumes, in the cases of the MAPSTM (on the left) and the NAPSTM (on the

right). We can see that the quality of the image is good in both cases, but an improvement with the MAPSTM is clearly visible on the places shown by red marks. On the top of the image, we can see the continuity of reflectors which was almost not visible in the case of the NAPSTM. On the bottom of the image, we can observe more details in the shape of the reflector in the case of the MAPSTM.

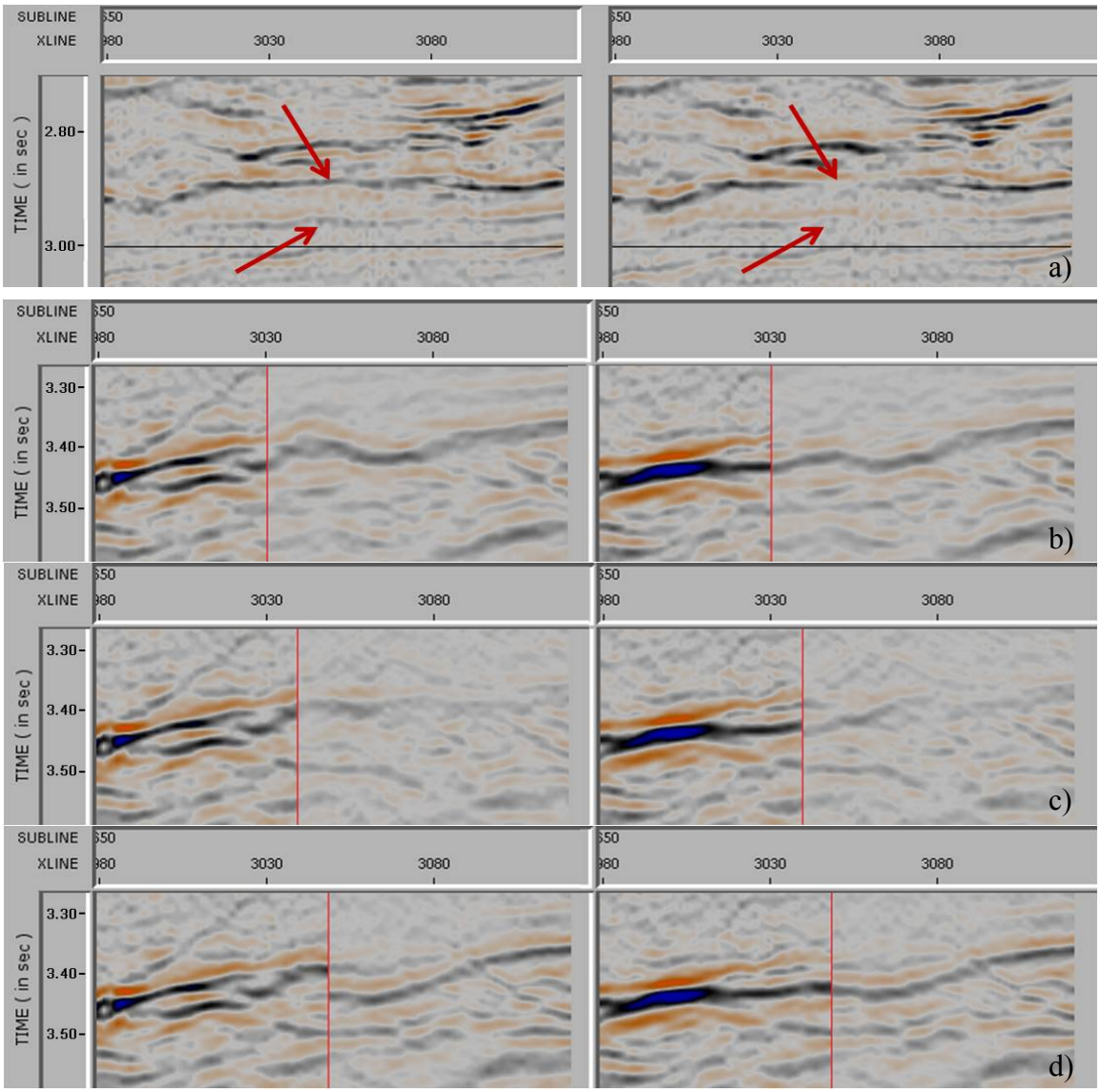

Figure 1 a) *Comparison of the MAPSTM (on the left) and the NAPSTM (on the right) for the three azimuths combined.* ***b)*** *Comparison between the combined azimuths and the azimuth 60° for the MAPSTM (on the left) and the NAPSTM (on the right).* ***c)*** *Comparison between the combined azimuths and the azimuth 120° for the MAPSTM (on the left) and the NAPSTM (on the right).* ***d)*** *Comparison between the combined azimuths and the azimuth 150° for the MAPSTM (on the left) and the NAPSTM (on the right). In figures b), c) and d), the combined azimuths are on the left hand-side of the red line on the stacked section, and the single azimuths are on the right.*

When comparing the same stacked sections for the three azimuths combined with the ones for a single azimuth, it appears that there is a shift for the reflectors in the case of the NAPSTM. This type of mismatch is discussed in more detail based on a synthetic example in Söllner et al. (2010). Figures 1-b,c,d show the comparison between the combined azimuths and the single ones (respectively 60°, 120°, and 150°) for the MAPSTM (on the left) and the NAPSTM (on the right). Following the same reflector in the case of the multi-azimuth prestack time migration, we can see that there is a very good match in the time position between the stacked sections for one azimuth and for the combined azimuth stack. In the case of the narrow-azimuth prestack time migration, we observe a shift in time

for some reflectors between the stacked sections for one azimuth and for the combined azimuths. This is particularly visible for the azimuths 120° and 150° (Figures 1-c and 1-d), along the strong reflector around 3.5s. These differences in the image time position of one and the same reflector for different azimuths, in the case of the NAPSTM, explain why the quality of the image after stacking all azimuths is at some places degraded.

Conclusions

In order to solve the mismatch problem which generally occurs when the data coming from different azimuths are stacked, a new method of multi azimuth prestack time migration has recently been developed (Söllner et al., 2010). Starting from the most general form of Hamilton's principal equation, an azimuthal time migration velocity function and a diffraction time function are built, valid for anisotropic and weakly heterogeneous media, for small and intermediate offsets.

In azimuthal velocity analysis, we split the diffraction time function in midpoint and offset dependent moveout terms and use for velocity updates only the offset dependent term, in migrated image gathers. From the updated velocities in three predominant azimuthal directions we built the velocity ellipse for the first run of MAPSTM. The resulting migrated gathers were stacked, or alternatively used in a second iteration of velocity analysis. The presented migration results from the Nile Delta multi-azimuth survey are based on one single velocity iteration. The same data were also processed with a narrow-azimuth prestack time migration, in order to assess the performance of MAPSTM. It appeared that the quality of the results was good in both cases. However, the resolution and structure delineation was generally better in MAPSTM, because the mismatch problem occurred in NAPSTM was solved and less destructive interferences were observed.

Acknowledgements

We highly acknowledge BP and RWE Dea for providing the data and for permission to publish this work. We thank our colleagues Konstantin Koch, and Seongbok Lee for help with data processing and software support.

References

Bortfeld, R. [1989] Geometrical ray theory: Rays and traveltimes in seismic systems (second-order approximations of the traveltimes). *Geophysics* **54**, 342-349.

Buchdahl, H.A. [1970] *An introduction to Hamiltonian Optics*. Dover Publications, New York.

Červený, V. [2001] *Seismic ray theory*. Cambridge University Press, Cambridge.

Grechka, V., Tsvankin, I. and Cohen, J.K. [1999] Generalized Dix equation and analytic treatment of normal-moveout velocity for anisotropic media. *Geophysical Prospecting*, **47**, 117-148.

Hubral, P. and Krey, T. [1980] *Interval Velocities from Seismic Reflection Time Measurements*. Society of Exploration Geophysicists, Tulsa, Oklahoma.

Hubral, P., Schleicher, J. and Tygel, M. [1992] Three-dimensional paraxial ray properties – Part I. Basic relations. *Journal of Seismic Exploration*, **1**, 265-279.

Keggin, J., Benson, M., Rietveld, W., Manning, T., Cook, P. and Page, C. [2007] Multi-azimuth 3D provides robust improvements in Nile Delta seismic imaging. *First Break*, **25**(3), 47-53.

Manning, T., Shane, N., Page, C., Barley, B., Rietveld, W. and Keggin, J. [2007] Quantifying and increasing the value of multi-azimuth seismic. *The Leading Edge*, **26**, 510-520.

Moser, T.J. and Červený, V. [2007] Paraxial ray methods for anisotropic inhomogeneous media. *Geophysical Prospecting*, **55**, 21-37.

Söllner, W., Tsvankin, I. and Silva, E.F.F. [2010] Multi-azimuth prestack time migration for anisotropic weakly heterogeneous media. *Journal of Seismic Exploration*, **19**, 187-206.

Ursin, B. [1982] Quadratic wavefront and traveltime approximations in inhomogeneous layered media with curved interfaces. *Geophysics*, **47**, 1012-1021.

van der Burg, D.W., Lin, S., Zhou, C. and Jiao, J. [2010]. Multi-azimuth high resolution tomography – Application to offshore Nile Delta. *72nd EAGE Conference & Exhibition*, Expanded Abstract B042.